AFRL-AFOSR-UK-TR-2016-0030

PHOTOSPHERIC DRIVING OF NON-POTENTIAL CORONAL MAGNETIC FIELD SIMULATIONS

Anthony Yeates
UNIVERSITY OF DURHAM

09/19/2016
Final Report

Air Force Research Laboratory
AF Office Of Scientific Research (AFOSR)/ IOE
Arlington, Virginia 22203
Air Force Materiel Command

REPORT DOCUMENTATION PAGE

Form Approved
OMB No. 0704-0188

1. REPORT DATE *(DD-MM-YYYY)*	2. REPORT TYPE	3. DATES COVERED *(From - To)*
26-10-2016	Final	15 Sep 2014 to 14 Sep 2017

4. TITLE AND SUBTITLE
PHOTOSPHERIC DRIVING OF NON-POTENTIAL CORONAL MAGNETIC FIELD SIMULATIONS

5a. CONTRACT NUMBER

5b. GRANT NUMBER
FA9550-14-1-0191

5c. PROGRAM ELEMENT NUMBER
61102F

6. AUTHOR(S)
Anthony Yeates

5d. PROJECT NUMBER

5e. TASK NUMBER

5f. WORK UNIT NUMBER

7. PERFORMING ORGANIZATION NAME(S) AND ADDRESS(ES)
UNIVERSITY OF DURHAM
STOCKTON ROAD
DURHAM, DH1 3LE GB

8. PERFORMING ORGANIZATION REPORT NUMBER

9. SPONSORING/MONITORING AGENCY NAME(S) AND ADDRESS(ES)
EOARD
Unit 4515
APO AE 09421-4515

10. SPONSOR/MONITOR'S ACRONYM(S)
AFRL/AFOSR IOE

11. SPONSOR/MONITOR'S REPORT NUMBER(S)
AFRL-AFOSR-UK-TR-2016-0030

12. DISTRIBUTION/AVAILABILITY STATEMENT
A DISTRIBUTION UNLIMITED: PB Public Release

13. SUPPLEMENTARY NOTES

14. ABSTRACT
The objective of this research is to develop a new photospheric driver to assimilate radial magnetic maps into magneto-frictional (MF) simulations of the Suns coronal magnetic field. Together with the Air Force Data Assimilative Photospheric Flux Transport (ADAPT) Model to assess how the MF model can improve background solar wind forecasts and whether flux ropes in the model can constrain magnetic topology or interplanetary magnetic fields. In the second year of the project improved filtering of magnetic maps was developed to reduce spurious electric fields. A new technique was developed for sparse reconstruction of electric field based on L1-minimization, which allowed a study of the effect of flux imbalance in magnetic maps. The PI and his associates published a description/proof-of-concept of the new MF driving technique, with test cases taken from (a) a simple flux transport model (with known electric field) and (b) a two-month ADAPT sequence. A comparison of different magnetic maps and coronal models was begun in collaboration with Predictive Science, Inc. This study focuses on how the differences affect solar wind predictions. The new MF code was used to assess potential benefits of placing a magnetograph at the L5 Lagrange point. This research developed the concept of field line helicity for robust identification of flux ropes in the corona. The results of these two studies has been published. Software was developed to automatically detect flux ropes using field line helicity, and tested on a previous MF model.

15. SUBJECT TERMS
Solar Magnetic Field

16. SECURITY CLASSIFICATION OF:			17. LIMITATION OF ABSTRACT	18. NUMBER OF PAGES	19a. NAME OF RESPONSIBLE PERSON
a. REPORT	b. ABSTRACT	c. THIS PAGE			MILLER, KENT
Unclassified	Unclassified	Unclassified	SAR	17	19b. TELEPHONE NUMBER *(Include area code)* 011-44-1895-616022

Standard Form 298 (Rev. 8/98)
Prescribed by ANSI Std. Z39.18

September 8, 2016

Award Number: **FA9550-14-1-0191**

Grant Title: **Photospheric Driving of Non-potential Coronal Magnetic Field Simulations**

PI Name: **Dr Anthony R. Yeates**

Department of Mathematical Sciences, Durham University, South Road, Durham DH1 3LE, UK
Tel: +44(0)191 334 3075 Email: anthony.yeates@durham.ac.uk

Period of performance: **15 Sep 2015 - 14 Sep 2016**

Contents

1 Summary **3**

2 Introduction **4**

3 Methods, Assumptions and Procedures **4**
3.1 MF model 4
3.2 Work Plan 6

4 Results and Discussion **7**
4.1 Year 2 Progress on Task 1 7
4.1.1 Filtering of magnetic maps 7
4.1.2 Sparse computation of electric field 8
4.1.3 Flux imbalance in magnetic maps 9
4.2 Year 2 Progress on Task 2 10
4.3 Year 2 Progress on Task 3 12
4.3.1 New collaboration: model comparison 12
4.3.2 Application to L5 mission 13
4.4 Year 2 Progress on Task 4 13
4.5 Resulting Presentations 14
4.6 Resulting Publications 15

5 Conclusions and Future Plans **16**

6 References **16**

7 List of Symbols, Abbreviations and Acronyms **17**

List of Figures

1 Longitudinally averaged current helicity density α (at $r \approx 1.03R_\odot$) as a function of latitude and time. 5

2 Example MF simulation of a simple bipolar active region. 6

3 The importance of smoothing of the input B_r maps. Top row shows the effect of smoothing a map of B_r. Middle and bottom rows show the effect of the smoothing on the reconstructed electric field, showing $-E_\theta$ and E_ϕ respectively. 8

4 Testing different electric field reconstructions on an analytical model of an emerging active region (in Cartesian coordinates). Top row shows the exact (target) solution for E_x, E_y and $\partial B_r/\partial t$. Middle row shows the inductive (curl free) electric field solution, showing clear long-range halos outside of the active region. Bottom row shows the result from L_1-minimization, which converges to the target solution. 9

5 Illustrating the effect of flux imbalance on the electric field. The left column shows $\partial B_z/\partial t$ where a new active region has only half appeared in the circular "assimilation region", so that the magnetic flux is imbalanced. The top row shows the resulting (L_1-minimum) electric field if an additive flux correction is subtracted from all pixels. It is not possible to localize $\mathbf{E}_h$ because the imbalance has been corrected globally. The bottom row shows the improved (but still imperfect) solution when a multiplicative flux correction is made (so that pixels with stronger B_r are corrected more). A better correction of the imbalance would have to account for the missing following polarity of the new active region. 10

6 A single sheared bipolar active region, after 600 hours evolution in the MF code [from 1]. The right image shows the original simulation (with imposed $\mathbf{E}_h$ on the surface), while the left and middle images show the simulation driven by reconstructed $\mathbf{E}_h$, with and without non-inductive correction for differential rotation, respectively. The flux rope is essentially absent at this time in the inductive-only simulation. 11

7 Globally integrated quantities for MF simulations based on ADAPT maps, showing the effect of different time cadences for the input maps [from 1]. Around hour 350, there is a significant drop in energy, associated with the re-assimilation of a significantly modified active region in the ADAPT maps. 12

8 Magnetic flux ropes identified using field line helicity ($\mathcal{A}$), for a snapshot of a MF simulation. Upper panel shows $\mathcal{A}$ on the solar surface, with flux rope footpoints identified by thresholding. Lower panel shows the resulting coronal flux ropes, projected on the solar surface. 14

1 Summary

Objective

The project is developing a new photospheric driver to assimilate radial magnetic maps into magneto-frictional (MF) simulations of the Sun's coronal magnetic field. It will be applied with the Air Force Data Assimilative Photospheric Flux Transport Model to assess how the MF model can improve background solar wind forecasts and whether flux ropes in the model can constrain ICME magnetic topology.

Executive summary of Year 2 Progress

- Developed improved filtering of magnetic maps to reduce spurious electric fields.
- Developed new technique for sparse reconstruction of electric field based on L_1-minimization, and studied the effect of flux imbalance in magnetic maps.
- Published a description/proof-of-concept of the new MF driving technique, with test cases taken from (a) a simple flux transport model (with known electric field) and (b) a two-month ADAPT sequence.
- Began comparison of different magnetic maps and coronal models, in collaboration with Predictive Science, Inc., focusing on how the differences affect solar wind predictions.
- Applied the new MF code to assess potential benefits of placing a magnetograph at the L5 Lagrange point, and published the results.
- Developed the concept of field line helicity for robust identification of flux ropes in the corona, and published a paper on its evolution in MF simulations.
- Developed software to automatically detect flux ropes using field line helicity, and tested on previous MF model.

2 Introduction

Forecasting the arrival at Earth of interplanetary coronal mass ejections (ICMEs) from the Sun relies on models both for the ICME propagation and for the background solar wind/interplanetary magnetic field (IMF). Both the ICME itself and the background IMF originate from and are driven by processes in the inner solar corona, below about 2.5 solar radii. Current operational forecasts by NOAA/SWPC combine the Wang-Sheeley-Arge-Enlil model for the coronal magnetic field/solar wind with a simple cone model for the ICME shape [2, 3]. However, the WSA model is based on a potential field extrapolation for the innermost layer of the corona. This model by definition cannot contain the twisted magnetic flux rope structures whose eruption is understood to initiate many ICMEs.

This project is developing a non-potential evolution model for the magnetic field in the inner corona (hereafter the MF – for magneto-frictional – model). By allowing for the build up and evolution of free magnetic energy in the low corona, the MF model (outlined in Section 3) offers two important possibilities: (i) improved modelling of the ambient IMF, and (ii) the opportunity to study the magnetic structure of erupting flux ropes. Self-consistent formation of twisted magnetic flux ropes in the coronal field is an important feature of the MF model. Moreover, these flux ropes can subsequently lose equilibrium and be ejected [4, 5].

In the wider context, several groups worldwide are developing full magnetohydrodynamic (MHD) simulations of the global solar corona [e.g., 6]. In comparison, the MF model simplifies the coronal evolution by (i) assuming a quasi-static evolution, and (ii) neglecting thermodynamic and gravitational effects. This simplification enables much longer integration times [for example, more than a solar cycle; 7], while retaining a continuous non-potential evolution of the magnetic field. In this respect, the MF model complements the full MHD simulations, in which it is too computationally expensive to study the build-up of free magnetic energy over periods of months to years. In essence, the MF model describes the formation of flux ropes (where and when will they form, and what will be their pre-eruptive structure). Full MHD models are required to accurately follow the eruptions themselves and to (directly) synthesize observable emission. In future, the computational speed of the MF model makes it a potential avenue for near-real time and/or ensemble forecasting of space weather.

3 Methods, Assumptions and Procedures

Here the basic MF model is summarised, before outlining the work plan that was proposed for this grant, and which is underway.

3.1 MF model

The mean magnetic field $\mathbf{B}$ in the coronal volume (typically $R_\odot < r < 2.5R_\odot$) is written in terms of a vector potential, $\mathbf{B} = \nabla \times \mathbf{A}$. This vector potential is evolved by the mean-field induction equation

$$\frac{\partial \mathbf{A}}{\partial t} = -\mathbf{E}, \tag{1}$$

where we use the Weyl gauge. The electric field is given by Ohm's law

$$\mathbf{E} = -\mathbf{v} \times \mathbf{B} + \mathbf{N}. \tag{2}$$

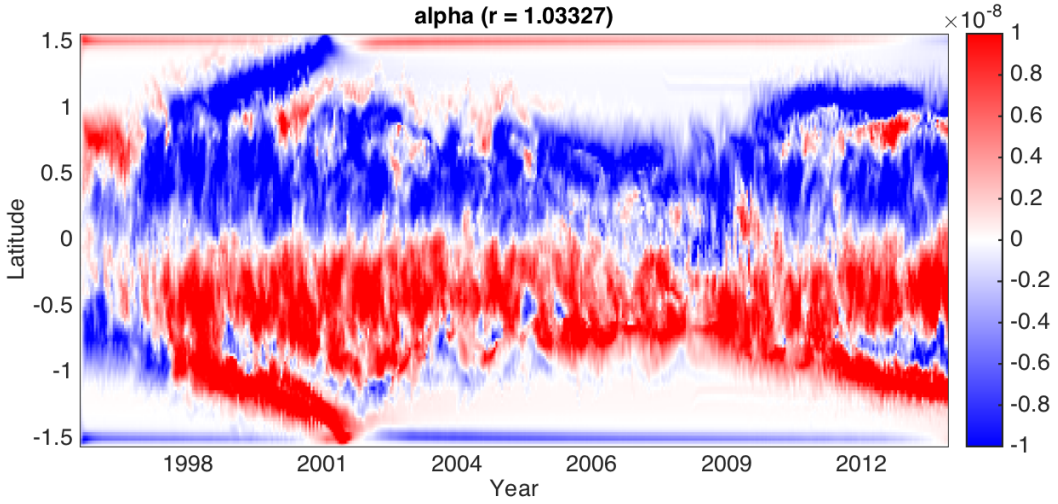

Figure 1: Longitudinally averaged current helicity density α (at $r \approx 1.03R_\odot$) as a function of latitude and time, in a continuous MF simulation running from 1996 to 2015 [updated from Ref. 7]. A clear hemispheric pattern is visible, and explaining how this is formed has been a success of the MF model [9].

In our model, the non-ideal term $\mathbf{N}$ describes not ohmic diffusion (which is negligible on large scales in the corona) but rather a "turbulent diffusion" arising from unresolved small-scale fluctuations. Following van Ballegooijen & Cranmer [8], we apply a hyperdiffusion

$$\mathbf{N} = -\frac{\mathbf{B}}{B^2}\nabla \cdot \left(\eta_4 B^2 \nabla \alpha\right), \tag{3}$$

where

$$\alpha = \frac{\mathbf{B}\cdot\mathbf{j}}{B^2} \tag{4}$$

is the current helicity density, with $\mathbf{j} = \nabla \times \mathbf{B}$ the current density. This form of hyperdiffusion preserves magnetic helicity density $\mathbf{A}\cdot\mathbf{B}$ in the volume and describes the tendency of the magnetic field to relax to a state of constant α, although such a state is never reached in global coronal simulations. Rather, the model produces a more complex nonlinear force-free magnetic structure where α is near constant along field lines but varies from one region to another. On a large scale, there is a hemispheric tendency in accordance with observations (Figure 1).

Rather than solving the full MHD momentum equation for the velocity $\mathbf{v}$, it is approximated with the form

$$\mathbf{v} = \frac{1}{\nu}\frac{\mathbf{j}\times\mathbf{B}}{B^2} + v_{\rm out}(r)\mathbf{e}_r. \tag{5}$$

The first term enforces relaxation of the magnetic field towards a (nonlinear) force-free state ($\mathbf{j}\times\mathbf{B} = 0$). Originally, the magneto-frictional method was introduced to compute individual force-free equilibria [10, 11]. Our approach differs in that B_r on the photospheric boundary is not held fixed, but provides a continuously varying input to drive the coronal field, which effectively evolves through a sequence of near force-free equilibria. The last term in Equation (5) is a radial outflow imposed only near the outer boundary ($r = 2.5R_\odot$) to represent the effect of the solar wind radially distending magnetic field lines [4].

At the photospheric boundary ($r = R_\odot$), $\nu \to \infty$ so that no friction is applied there and magnetic field lines are tied to the motion of their photospheric footpoints. On this boundary,

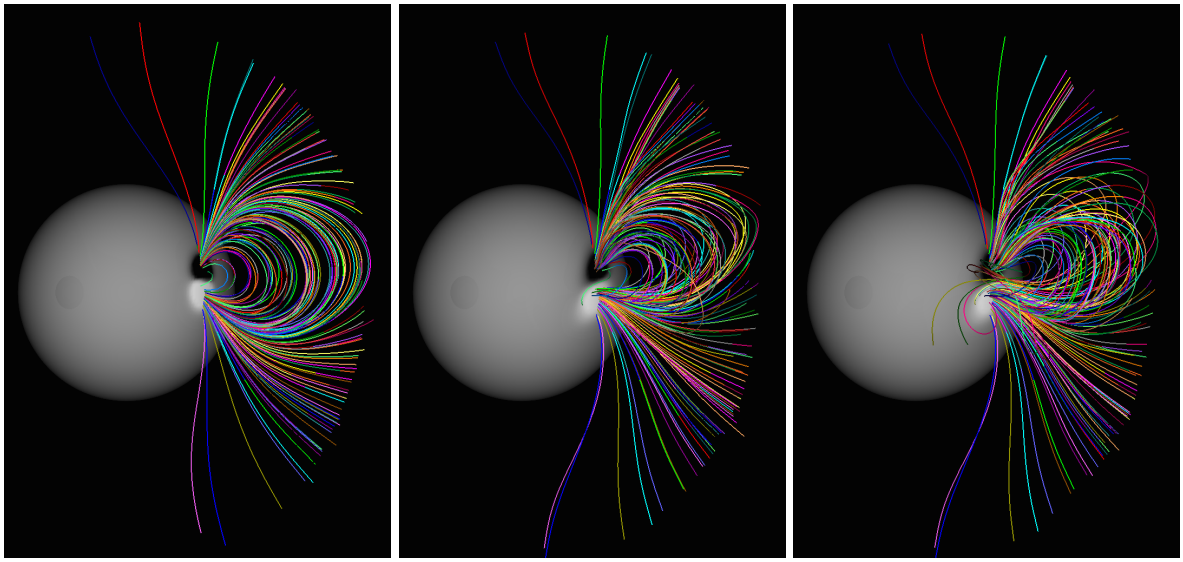

Figure 2: Example MF simulation of a simple bipolar active region. After 25 days (middle) a flux rope has formed under the sheared arcade above the polarity inversion line. After 27 days (right) the flux rope has lost equilibrium and is being ejected through the outer boundary. No magnetic flux emerges through the photosphere during this simulation; the flux rope is formed purely by footpoint shearing (through differential rotation) and flux cancellation at the inversion line. Note that the Sun is rotated so that north is to the left in these images.

boundary conditions are required for the horizontal electric field $\mathbf{E}_h$ (i.e., the components E_θ, E_ϕ), as a function of time. In our previous simulations, we have chosen $\mathbf{E}_h$ according to a surface flux transport model with specified large scale flows and supergranular diffusion. New active regions were emerged through the insertion of idealised magnetic bipoles, with shape and size chosen to match observed active regions [12, 13]. The subsequent 3d evolution of one such bipole is shown in Figure 2. This procedure had two limitations: firstly, it limited the accuracy with which we could reproduce the structure of real active regions, particularly those of a complex multipolar structure. Secondly, the new bipoles were determined from synoptic magnetic maps, meaning that each longitude on the Sun was updated only once per 27-day carrington rotation. This limited the time evolution of the model.

3.2 Work Plan

This project seeks to develop a new numerical routine to assimilate radial magnetic maps into the MF model, replacing the previous simplified flux transport model. It will be used to drive MF simulations using high-resolution radial field maps generated by the Air Force Data Assimilative Photospheric Flux Transport Model (ADAPT). The proposed work plan was comprised of five tasks:

1. Develop numerical code to drive the magneto-frictional model using a sequence of radial field maps on the photospheric boundary.

2. Test the code with ADAPT radial field maps to determine (i) the optimum time resolution for assimilation of the maps, and (ii) the effect on coronal outputs compared to the simpler

bipole driver used previously with the MF model. At this stage, the PI, PDRA and DHM will visit AFRL (where ADAPT is developed).

3. Apply the combined ADAPT-MF code to quantify ambient solar wind properties. In particular, how does the predicted open field structure and solar wind speed differ from the potential-field based Wang-Sheeley-Arge model?

4. Analyse the magnetic flux ropes in the ADAPT-MF simulations, to determine how the distribution of flux ropes and their eruption rate differs from the earlier simulations with simple bipole driver. Also compute statistics of the magnetic flux and current helicity content of the flux ropes.

5. Assess the uncertainty in coronal outputs due to possible patterns of photospheric helicity injection.

4 Results and Discussion

In this section, we describe the progress made in Year 2 of the project.

4.1 Year 2 Progress on Task 1

In Year 1 we implemented numerical code to compute the horizontal electric field $\mathbf{E}_h$ based on a time sequence of radial magnetic field maps. In Year 2, this code has been fully tested and written up (see Section 4.2). However, we have continued to investigate improved methods of electric field reconstruction, which are briefly described here. The overall aim is to reduce spurious electric fields that result from errors in the reconstruction, so as to give a good estimate of the true electric field.

The true electric field will obey (approximately) the ideal Ohm's law $\mathbf{E} = -\mathbf{v} \times \mathbf{B}$, where $\mathbf{v}$ is the plasma velocity. However, since our data is limited to B_r, our reconstruction of $\mathbf{E}_h$ is based only on partial information. In general, it will not be possible to reconstruct $\mathbf{E}_h$ uniquely, but with suitable physical assumptions it is possible to choose a more plausible solution.

4.1.1 Filtering of magnetic maps

We have found that both spatial and temporal smoothing of the input B_r maps are necessary. In effect, temporal smoothing amounts to using more than just two successive maps to estimate $\partial B_r/\partial t$. In practice, we implement a quadratic Savitsky-Golay smoothing filter. The window size (number of maps) is chosen so as minimize $\int |\mathbf{E}_h| \, \mathrm{d}S$ (typically 9 or 11 maps).

The improvement is illustrated in Figure 3. It is seen that the temporal filter removes strong electric fields outside of active regions, while maintaining the large-scale magnetic field distribution. In effect, we are removing small-scale changes in B_r that are uncorrelated from one map to the next. These correspond to fast, small-scale motions that cannot be resolved for our given cadence of input maps. The uncorrelated changes lead to significant electric fields that do not represent the true evolution. If left in, these would produce unrealistic results in the MF simulations.

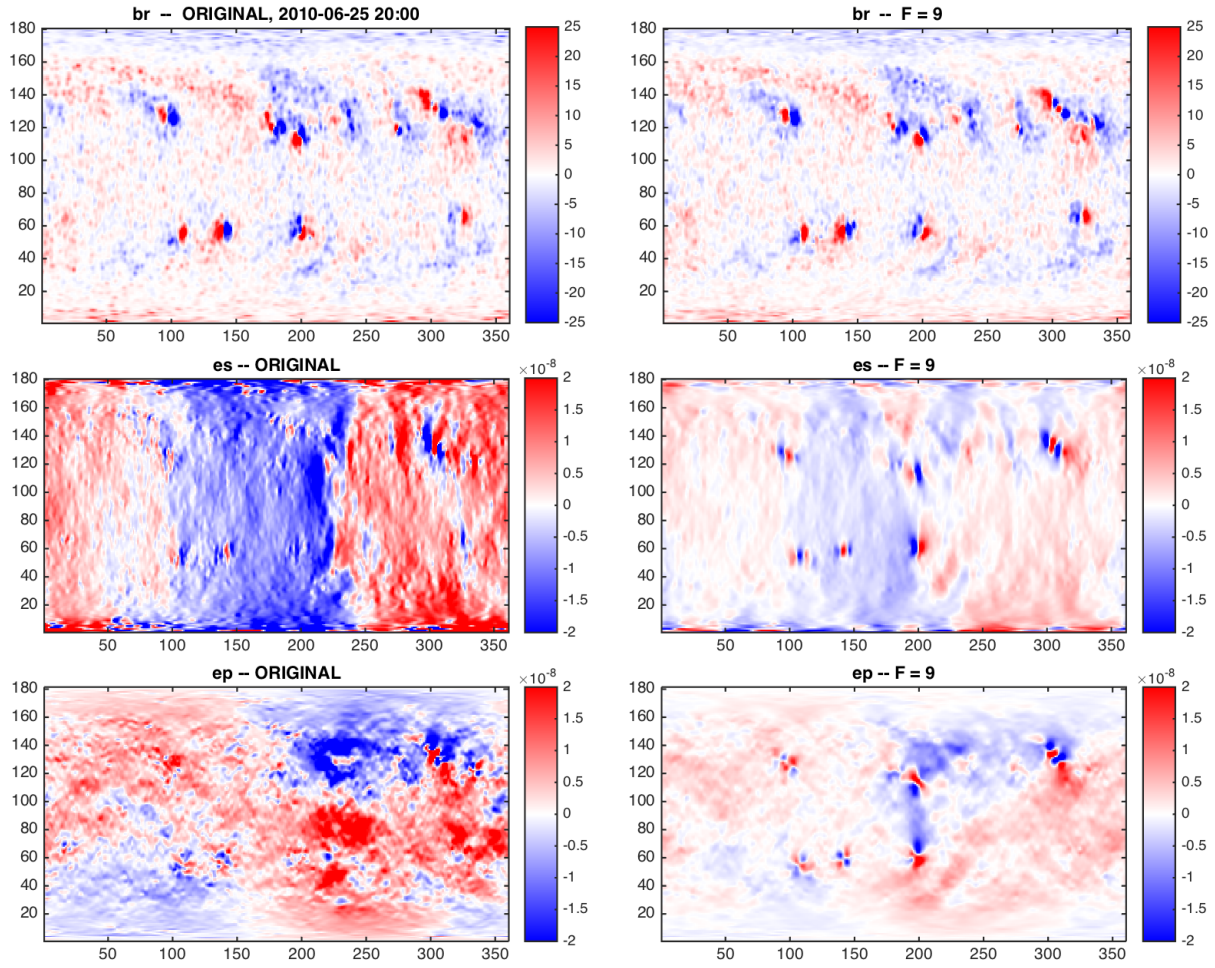

Figure 3: The importance of smoothing of the input B_r maps. Top row shows the effect of smoothing a map of B_r. Middle and bottom rows show the effect of the smoothing on the reconstructed electric field, showing $-E_\theta$ and E_ϕ respectively.

4.1.2 Sparse computation of electric field

A second area of ongoing research concerns how to choose the non-inductive (curl free) part of $\mathbf{E}_h$. This is unconstrained by the B_r maps, but comparable in magnitude to the inductive part when $\mathbf{E}_h$ arises from Ohm's law. In Year 1, we implemented a method of determining the non-inductive contribution from differential rotation, based on a known velocity profile [1]. However, we noted a problem with electric field "halos" arising from regions of strong $\partial B_r/\partial t$, such as when new active regions are assimilated into the ADAPT model. The halos represent a spurious long-range electric field that is absent in reality, since Ohm's law causes the electric field to be localised within the active region. In reality, there is a non-inductive part of $\mathbf{E}_h$ that cancels the halo.

In Year 2, we have developed a new approach to computing "sparse" (localised) electric fields, based on L_1-minimisation. The idea is to find an electric solution that minimises $\int |\mathbf{E}_h| \, \mathrm{d}S$, using variational methods. In the optimization literature, this is known as "basis pursuit", and in most cases will coincide with the sparsest solution to the given system (fewest non-zero entries). This solution should have no non-essential halos. A refinement that im-

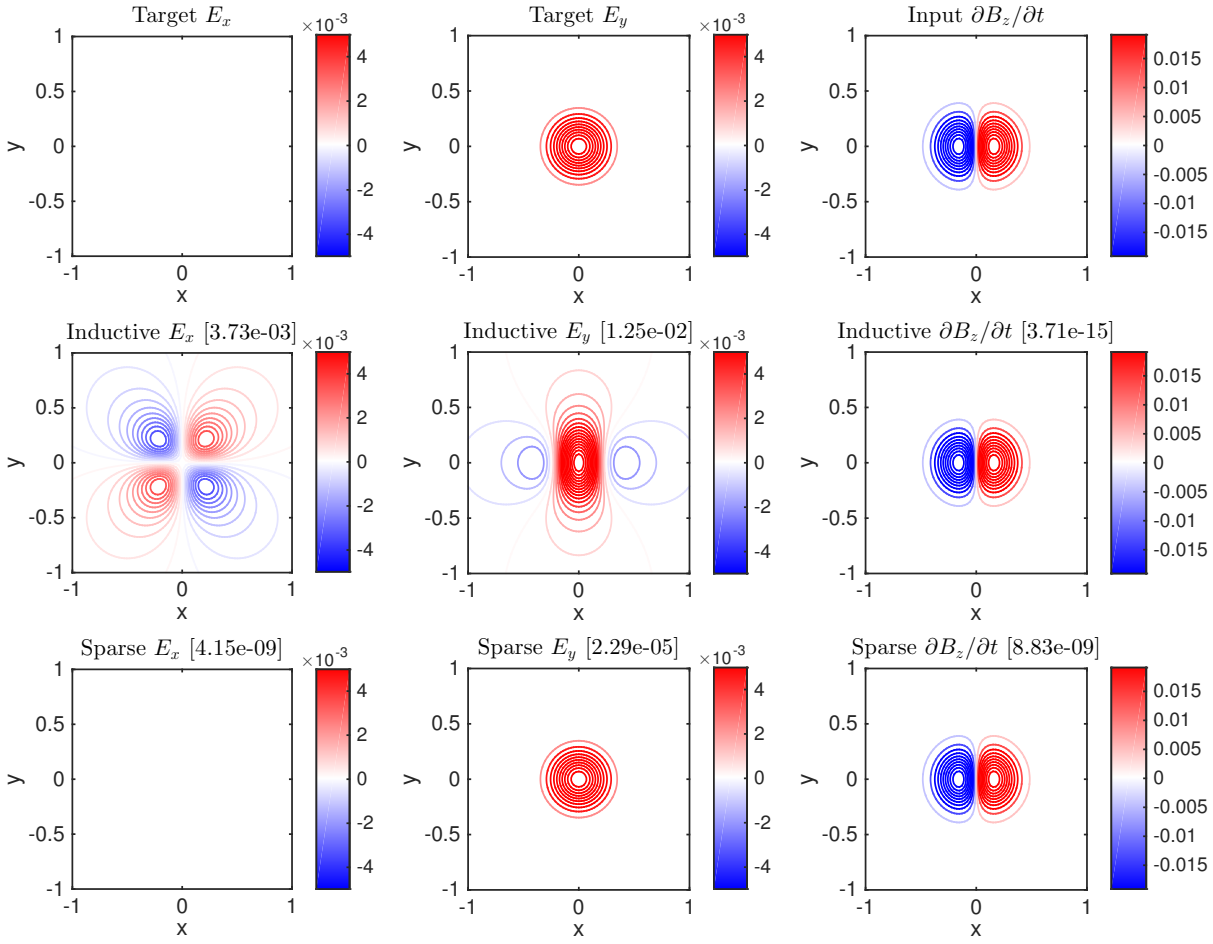

Figure 4: Testing different electric field reconstructions on an analytical model of an emerging active region (in Cartesian coordinates). Top row shows the exact (target) solution for E_x, E_y and $\partial B_r/\partial t$. Middle row shows the inductive (curl free) electric field solution, showing clear long-range halos outside of the active region. Bottom row shows the result from L_1-minimization, which converges to the target solution.

proves the smoothness of solutions is to minimize a linear combination of the L_1 and L_2 norms (called L_1-penalized least-squares). These methods are capable of producing smoother and more realistic electric fields than the L_0 minimization tried in Year 1.

We have developed some simple analytical models for testing these various electric field reconstructions. An example, representing the emergence of a bipolar active region, is shown in Figure 4. This example uses a Cartesian grid, but the methods have also been implemented in spherical geometry and applied to the ADAPT maps. A paper describing the sparse reconstruction of electric fields is in preparation, as it is believed that this will be of interest to the wider community.

4.1.3 Flux imbalance in magnetic maps

One aspect of the project is to assess the limitations of ADAPT maps for driving global coronal simulations such as MF, and in particular to suggest areas for improvement. A good example

is the imbalance between positive and negative magnetic flux in the ADAPT maps. This results from the fact that magnetogram data is (necessarily) assimilated over only part of the map, so that the assimilated flux may be unbalanced. When used to drive the simulations, this imbalance must be corrected so that there is no net magnetic flux through the solar surface. As illustrated in Figure 5, when this imbalance is large it can significantly affect the electric field, even at large distances from the region of imbalance. This work suggests that careful correction of flux imbalance would improve the accuracy of coronal simulations. In particular, imbalances ought to be corrected as locally as possible in the magnetic maps. Ideally, this would be done during construction of future generations of ADAPT maps.

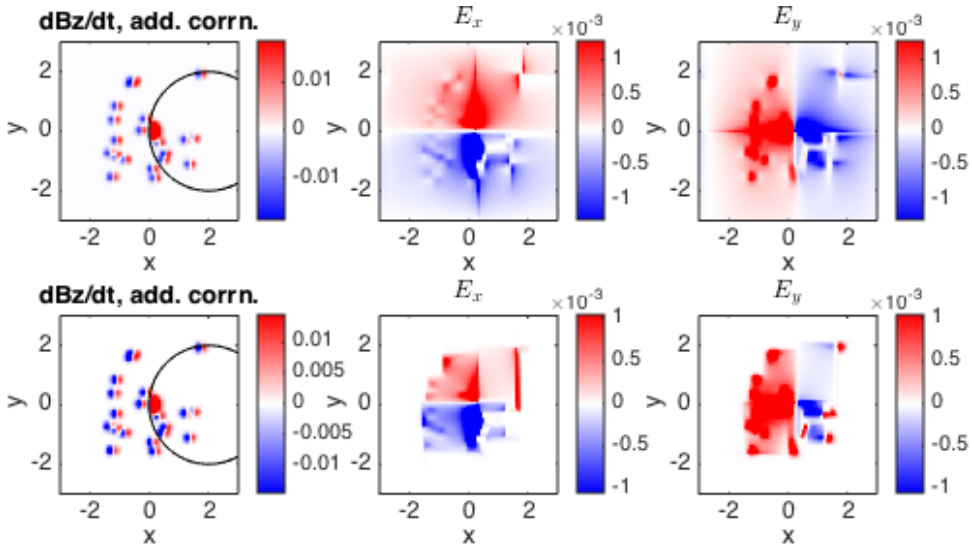

Figure 5: Illustrating the effect of flux imbalance on the electric field. The left column shows $\partial B_z/\partial t$ where a new active region has only half appeared in the circular "assimilation region", so that the magnetic flux is imbalanced. The top row shows the resulting (L_1-minimum) electric field if an additive flux correction is subtracted from all pixels. It is not possible to localize $\mathbf{E}_h$ because the imbalance has been corrected globally. The bottom row shows the improved (but still imperfect) solution when a multiplicative flux correction is made (so that pixels with stronger B_r are corrected more). A better correction of the imbalance would have to account for the missing following polarity of the new active region.

4.2 Year 2 Progress on Task 2

We have published details of the technique for driving MF simulations with ADAPT maps [1]. Since the true electric field is unknown in ADAPT, we also simulated a series of magnetic maps from a simpler flux transport model with known electric field. The simplest example modelled the shearing of a single bipolar active region by differential rotation, forming a single twisted flux rope which loses equilibrium and is ejected. This example highlighted the importance of the non-inductive electric field for building up sheared fields inside active regions (Figure 6). A purely inductive $\mathbf{E}_h$ delayed the eruption of the flux rope by 21 days. Our conclusion is that the electric field driving technique is able to reproduce the results of previous MF simulations provided that the non-inductive electric field is accounted for, at least to leading order.

The ADAPT-driven simulations described by Weinzierl et al. [1] cover a two-month test

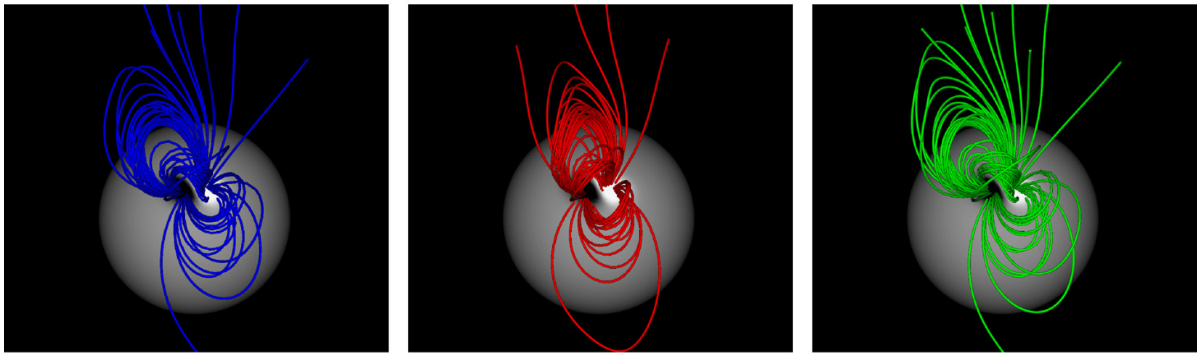

(d) Improved, hour 600 (e) Inductive-only, hour 600 (f) Original, hour 600

Figure 6: A single sheared bipolar active region, after 600 hours evolution in the MF code [from 1]. The right image shows the original simulation (with imposed $\mathbf{E}_h$ on the surface), while the left and middle images show the simulation driven by reconstructed $\mathbf{E}_h$, with and without non-inductive correction for differential rotation, respectively. The flux rope is essentially absent at this time in the inductive-only simulation.

period in November-December 2014. Some globally integrated quantities are shown in Figure 7, while further details are given in the paper. The main conclusions are:

1. Time sequences of ADAPT maps can be successfully and stably used to drive MF simulations of the coronal magnetic field.

2. Within the range of 2-24 hours, global quantities in the simulation are not very sensitive to the time cadence between input maps. However, the local structure of magnetic flux ropes can sometimes be altered, particularly if temporal filtering of the input maps is too weak.

3. For the ADAPT maps, the non-inductive correction for differential rotation does not have a significant effect on the globally integrated quantities (Figure 7). However, this may mask differences in the local structure of the field that can lead to differences in flux rope formation times and loss of equilibrium.

4. The data assimilation can lead to strong electric fields, and halos. There was a good example in this test period, where a large active region was re-assimilated with significantly changed structure. In reality, the change would have occurred during a 14-day period while the region was on the far side of the Sun. Sudden changes in the photospheric B_r like this lead to disconnection of flux in the MF simulation. This horizontal magnetic field is subsequently ejected out of the top of the simulation box, accounting for the peak in open magnetic flux seen in Figure 7. It is likely that the region did not evolve in this precise way in reality, although it would still have needed to shed magnetic flux. This suggests that simulation results near to the East limb must be treated with care, as they may show transient behaviour linked to the data assimilation.

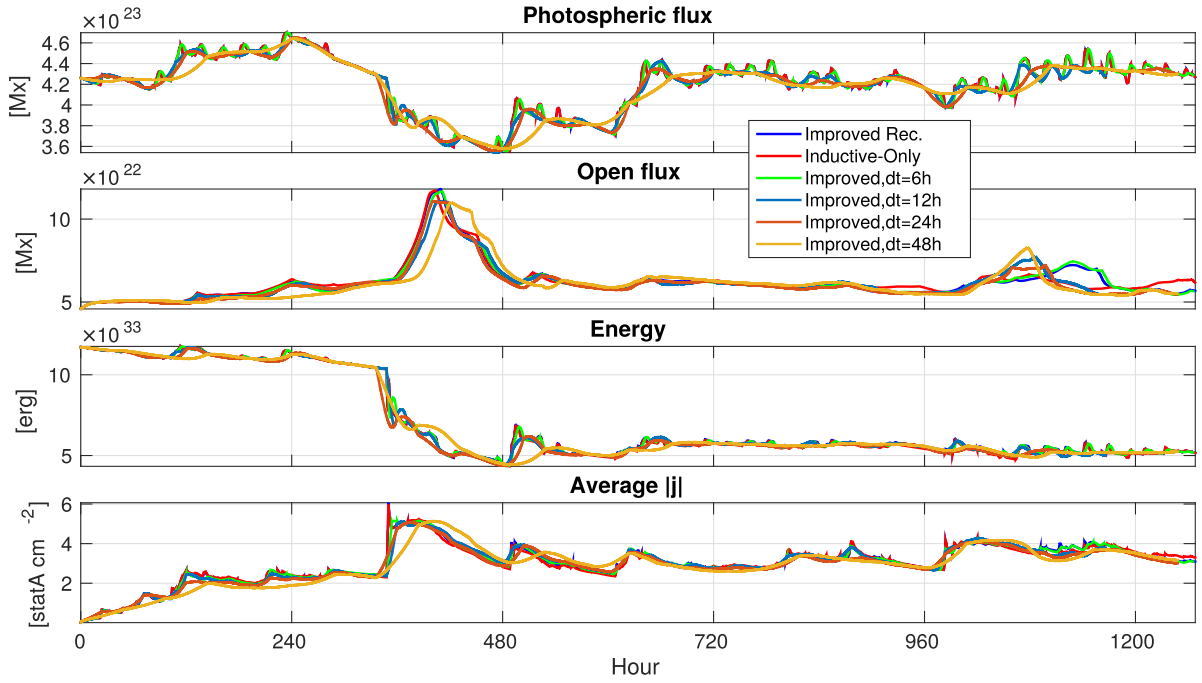

Figure 7: Globally integrated quantities for MF simulations based on ADAPT maps, showing the effect of different time cadences for the input maps [from 1]. Around hour 350, there is a significant drop in energy, associated with the re-assimilation of a significantly modified active region in the ADAPT maps.

4.3 Year 2 Progress on Task 3

4.3.1 New collaboration: model comparison

Co-Is Arge and Henney, along with PI Yeates and J. Linker, ran a session on "Coronal Magnetic Maps" at the 2016 SHINE meeting in Santa Fe, New Mexico. The session brought together makers of magnetic field maps with coronal modellers, to compare the effect of different input maps on coronal and solar wind model results. As part of the exercise (which is intended to be published in due course), we ran MF simulations for the challenge data (2010 July 8) based both on ADAPT maps and the Lockheed Martin flux transport model.

We found that the MF model enhanced the open magnetic flux compared to potential-field models, with a similar effect to lowering the source surface in the potential fields to $2R_\odot$. This enhancement was less than that in MHD simulations, and well below the level inferred from OMNI data. It is possible that longer MF simulations (integration time was limited to 3 months), or those incorporating additional helicity injection (task 5) could increase the open flux further. We also found that the MF model perturbed the position of the heliospheric current sheet; along with changes in coronal magnetic topology, this could significantly affect predicted wind speeds at Earth.

An important finding from this exercise was that, in order to reproduce the observed level of open flux in either MHD or MF models, the corresponding open flux footpoints on the solar surface would have to be much larger than the coronal holes observed in extreme-ultraviolet. This was an unequivocal result from all of the magnetic maps.

4.3.2 Application to L5 mission

A spin-off application of our new MF code has been to assess the potential benefits from placing a magnetograph at the L5 Lagrange point. In this case, the simulations were driven by a sequence of NSO magnetograms, along with a sequence where two active regions were observed "earlier" to mimick the availability of observations from L5. We found that differences within the active regions persist for several days after the region is observed from both L5 and Earth. However, differences in the long-range connectivity of the active region (e.g. the open magnetic flux) were found to persist for much longer, indicating that L5 observations could potentially provide an important improvement for space weather forecasting. This work has been accepted for publication in *Astrophys. J.* (Weinzierl et al.).

4.4 Year 2 Progress on Task 4

In Year 2, we have begun work on Task 4 by developing new methods to identify magnetic flux ropes, and to measure their flux and helicity content. The results will be used to carry out large-scale studies based on longer MF simulations in Year 3.

We began with a critical analysis of the method used by Yeates & Mackay [5] to detect flux ropes in simulated coronal magnetic fields, which was based on testing the Lorentz force at grid points in the volume. This method did not assign an accurate volume to each rope, and so an alternative was needed in order to measure quantities such as magnetic flux or helicity of the rope.

We have developed an alternative method to detect (and define) flux ropes based on field line integration. This has taken advantage of the fast routines for magnetic field-line integration developed for Task 3 in Year 1. Using magnetic field lines to identify flux ropes is a natural idea, since the usual definition of a flux rope is a twisted bundle of field lines. In addition, this method gives us (automatically) the footpoints of the flux rope, allowing straightforward computation of the flux and tracking of the rope's evolution.

After experimenting with quantities based on the parallel electric current and local twist of the field line, we have settled on an alternative quantity called the "field line helicity" for defining flux ropes. For a given magnetic field line, this is defined as the integral of the magnetic vector potential along that field line. This is effectively a density of magnetic helicity per field line, and is an ideal invariant provided the field line endpoints are fixed. In our case, the endpoints are moving due to the electric field on the solar surface, so helicity is injected over time. In this case, some care needs to be taken with the gauge of the vector potential — a suitable choice is described in our recent paper that is currently in press in *Astron. Astrophys.* (Yeates & Hornig).

Figure 8 shows the flux ropes detected on a particular day by thresholding the field line helicity. As a topological quantity, the field line helicity can robustly determine twisted magnetic structures. It measures only topologically "essential" structures (that cannot be undone by an ideal relaxation), and is thus more robust than measures based on local twist. For a comparison, see the paper by Yeates & Hornig. A fast numerical code has been implemented for computing field line helicity in the MF simulations, and we are currently testing the method on a long simulation driven by a simple flux transport model, before applying it to ADAPT-driven simulations. A paper describing the method and initial results is in preparation.

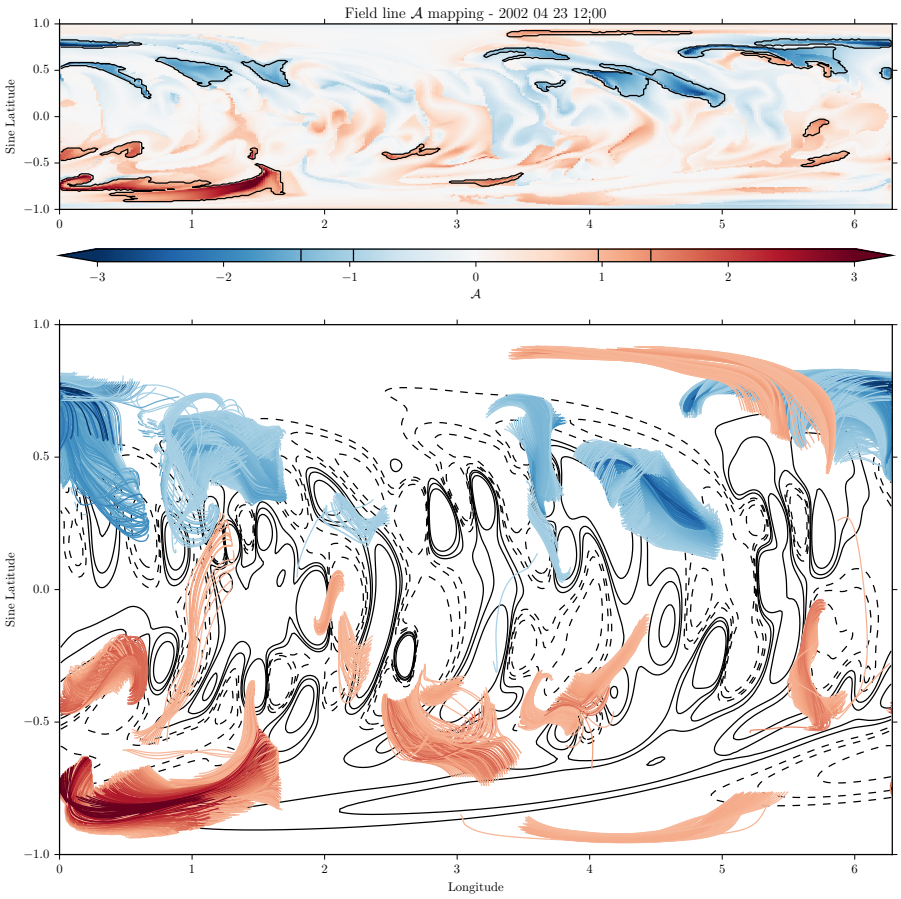

Figure 8: Magnetic flux ropes identified using field line helicity ($\mathcal{A}$), for a snapshot of a MF simulation. Upper panel shows $\mathcal{A}$ on the solar surface, with flux rope footpoints identified by thresholding. Lower panel shows the resulting coronal flux ropes, projected on the solar surface.

4.5 Resulting Presentations

1. *Reconstruction of Photospheric Electric Fields from Line-of-sight Magnetograms for Driving of Non-potential Solar Corona Simulations*, Met Office-Air Force-Durham meeting, Exeter, 17-Nov-15 [Weinzierl].

2. *Detection and characterisation of solar magnetic flux ropes*, Met Office-Air Force-Durham meeting, Exeter, 17-Nov-15 [Lowder].

3. *Connecting coronal holes and open magnetic flux through observation and models of solar cycles 23 and 24* [Lowder],

   - RAS specialist discussion meeting on automated data analysis in solar physics, London, 8-Jan-16.
   - seminar, Northumbria, 20-Apr-16.

4. *Automated detection of magnetic flux ropes*, RAS specialist discussion meeting on automated data analysis in solar physics, London, 8-Jan-16 [Yeates].

5. *A New Technique for the Photospheric Driving of Non-Potential Solar Coronal Magnetic Field Simulations*, seminar, St Andrews, 11-May-16 [Weinzierl].
6. *Magnetic flux rope identification and characterization from observationally-driven solar coronal models* [Lowder],
   - UKMHD meeting, Glasgow, 12-May-16.
   - National Astronomy meeting, Nottingham, 28-Jun-16.
7. *The global distribution of magnetic helicity in the Sun's corona* [Yeates],
   - seminar, Durham, 17-Mar-16.
   - IUTAM symposium on helicity structures and singularity in fluid and plasma dynamics, Italy, 11-Apr-16.
   - UKMHD meeting, Glasgow, 12-May-16.
   - CFSA seminar, Warwick, 6-Jun-16.
   - SHINE workshop, New Mexico, 11-Jul-16.
8. *Photospheric driving of non-potential coronal magnetic field simulations*, Bz workshop, New Mexico, 18-Jul-16 [Yeates].
9. *Magneto-frictional models and electric fields*, LWS working group meeting, St Andrews, 14-Aug-16 [Yeates].
10. *Magneto-frictional simulations of flux rope formation and eruption*, LWS working group meeting, St Andrews, 14-Aug-16 [Lowder].

4.6 Resulting Publications

1. Edwards, S.J., Yeates, A.R., Bocquet, F.-X., & Mackay, D.H., Influence of non-potential coronal magnetic field topology on solar-wind models, *Solar Phys.* **290**, 2791 (2015).
2. Weinzierl, M., Yeates, A.R., Mackay, D.H., Henney, C.J., & Arge, C.N., A new technique for the photospheric driving of non-potential solar coronal magnetic field simulations, *Astrophys. J.* **823**, 55 (2016).
3. Yeates, A.R. & Hornig, G., The global distribution of magnetic helicity in the solar corona, *Astron. Astrophys.* (in press), http://arxiv.org/abs/1606.06863.
4. Weinzierl, M., Mackay, D.H., Yeates, A.R., & Pevtsov, A.A., The possible impact of L5 magnetograms on non-potential coronal magnetic field simulations, *Astrophys. J.* (in press).

In preparation:

1. Yeates, A.R., Sparse reconstruction of electric fields from radial magnetic data.
2. Lowder, C. & Yeates, A.R., Magnetic flux rope identification and characterization from observationally-driven solar coronal models.

5 Conclusions and Future Plans

In summary, significant progress has now been made on four of the five tasks in the project. Imminent work will involve publishing our new methods for sparse electric field reconstruction and flux rope identification. With our preliminary tests and techniques in place, we plan to begin longer ADAPT-driven simulations (several years) in the fall. This will allow us to assess the long-term behaviour of different electric field reconstructions, and also to compare the background solar wind (task 3) with the potential-field model. It will also allow us to study the statistics of magnetic flux ropes. We will also run simulations with different parametrizations of small-scale helicity injection, in order to address task 5.

In Year 3, postdoc Lowder will continue to work on analysis of flux ropes, and postdoc Weinzierl will focus on running the ADAPT-MF simulations and studying the impact on solar wind outputs. With this in mind, Weinzierl has recently been working on optimizing the WSA empirical solar wind model for the MF code. PI Yeates will concentrate on finalizing the electric field computation, documenting the final-form of the MF code, and directing the overall project to a successful conclusion.

6 References

[1] M. Weinzierl, A. R. Yeates, D. H. Mackay, C. J. Henney, C. N. Arge, A New Technique for the Photospheric Driving of Non-potential Solar Coronal Magnetic Field Simulations, *Astrophys. J.* **823**, 55 (2016).

[2] V. Pizzo, *et al.*, Wang-sheeley-arge-enlil cone model transitions to operations, *Space Weather* **9**, S03004 (2011).

[3] C. O. Lee, *et al.*, Ensemble modeling of CME propagation, *Solar Phys.* **285**, 349 (2013).

[4] D. H. Mackay, A. A. van Ballegooijen, Models of the Large-Scale Corona. I. Formation, Evolution, and Liftoff of Magnetic Flux Ropes, *Astrophys. J.* **641**, 577 (2006).

[5] A. R. Yeates, D. H. Mackay, Initiation of coronal mass ejections in a global evolution model, *Astrophys. J.* **699**, 1024 (2009).

[6] R. Lionello, J. A. Linker, Z. Mikić, Multispectral Emission of the Sun During the First Whole Sun Month: Magnetohydrodynamic Simulations, *Astrophys. J.* **690**, 902 (2009).

[7] A. R. Yeates, D. H. Mackay, Chirality of high-latitude filaments over solar cycle 23, *Astrophys. J.* **753**, L34 (2012).

[8] A. A. van Ballegooijen, S. R. Cranmer, Hyperdiffusion as a Mechanism for Solar Coronal Heating, *Astrophys. J.* **682**, 644 (2008).

[9] A. R. Yeates, D. H. Mackay, Modelling the global solar corona: III. origin of the hemispheric pattern of filaments, *Solar Phys.* **254**, 77 (2009).

[10] W. H. Yang, P. A. Sturrock, S. K. Antiochos, Force-free magnetic fields - The magneto-frictional method, *Astrophys. J.* **309**, 383 (1986).

[11] I. J. D. Craig, A. D. Sneyd, A dynamic relaxation technique for determining the structure and stability of coronal magnetic fields, *Astrophys. J.* **311**, 451 (1986).

[12] A. R. Yeates, D. H. Mackay, A. A. van Ballegooijen, Modelling the global solar corona: Filament chirality observations and surface simulations, *Solar Phys.* **245**, 87 (2007).

[13] A. R. Yeates, D. H. Mackay, A. A. van Ballegooijen, Modelling the global solar corona II: coronal evolution and filament chirality comparison, *Solar Phys.* **247**, 103 (2008).

7 List of Symbols, Abbreviations and Acronyms

- $\mathbf{A}$: vector potential
- ADAPT: Air Force Data-Assimilative Photospheric flux Transport model
- α: current helicity density $alpha = \mathbf{j} \cdot \mathbf{B}/B^2$
- $\mathbf{B}$: magnetic field
- $\mathbf{E}$: electric field (the horizontal part is denoted $\mathbf{E}_h$)
- ICME: interplanetary coronal mass ejection
- IMF: interplanetary magnetic field
- $\mathbf{j}$: current density
- MF model: magneto-frictional model
- MHD: magnetohydrodynamics
- NSO: National Solar Observatory
- $\mathbf{v}$: velocity field
- WSA: Wang-Sheeley-Arge model for the solar wind